HHS Public Access

Author manuscript

Adv Biol Regul. Author manuscript; available in PMC 2025 January 15.

Published in final edited form as:

Adv Biol Regul. 2023 December ; 90: 100990. doi:10.1016/j.jbior.2023.100990.

PHOSPHORYLATION IMPACTS GLE1 NUCLEAR LOCALIZATION AND ASSOCIATION WITH DDX1

Manisha Sharma[*], **Aaron C. Mason**[*], **T. Renee Dawson**[*], **Susan R. Wente**[^]

[*]Department of Cell and Development Biology, School of Medicine, Vanderbilt University, Nashville, TN, USA

[^]Department of Biology, and Biochemistry, Wake Forest University, Winston-Salem, NC, USA

Abstract

Gle1 regulates gene expression at multiple steps from transcription to mRNA export to translation under stressed and non-stressed conditions. To better understand Gle1 function in stressed human cells, specific antibodies were generated that recognized the phosphorylation of threonine residue 102 (T102) in Gle1. A series of *in vitro* kinase assays indicated that T102 phosphorylation serves as a priming event for further phosphorylation in Gle1's N-terminal low complexity cluster. Indirect immunofluorescence microscopy with the anti-Gle1-pT102 antibodies revealed that basally phosphorylated Gle1 was pre-dominantly nuclear with punctate distribution; however, under sodium arsenite-induced stress, more cytoplasmic localization was detected. Immunoprecipitation with the anti-Gle1-pT102 antibody resulted in co-isolation of Gle1-pT102 with the DEAD-box protein DDX1 in a phosphatase sensitive manner. This suggested Gle1 phosphorylation might be linked to its role in regulating DDX1 during transcription termination. Notably, whereas the total Gle1-DDX1 association was decreased when Gle1 nucleocytoplasmic shuttling was disrupted, co-isolation of Gle1-pT102 and DDX1 increased under the same conditions. Taken together, these studies demonstrated that Gle1 phosphorylation impacts its cellular distribution and potentially drives nuclear Gle1 functions in transcription termination. We propose a model wherein phosphorylation of Gle1 either reduces its nucleocytoplasmic shuttling capacity or increases its binding affinity with nuclear interaction partners.

Keywords

phosphorylation; Gle1; DDX1

Introduction

During synthesis, an mRNA transcript is assembled with RNA-binding proteins (RBPs) to form a messenger ribonucleoprotein complex (mRNP). Dynamic exchange of specific

Declarations of interest: none

RBPs within this complex direct both the subcellular trafficking of an mRNP and its interactions with cellular machinery, determining its fate from transcription to translation to decay (Bohnsack et al., 2023; Natalizio and Wente, 2013). This is particularly the case for DEAD box proteins (DBPs) that bind to and alter mRNPs through ATPase-dependent torsional force or helicase activity. For example, DDX1, DDX5, DHX9 and Senataxin (SET-X) unwind DNA:RNA hybrids (R-loops) formed during transcription termination (Chakraborty et al., 2018; Mersaoui et al., 2019; Skourti-Stathaki et al., 2011). Likewise, DDX1 associates with the transcript and transcription termination machinery to coordinate pre-mRNA cleavage (Bléoo et al., 2001; Sharma and Wente, 2020). In later stages of mRNP maturation, the highly conserved member of the TREX complex UAP56/DDX39 (*S. cerevisiae* Sub2) is required to direct Exon-Junction complex formation and pre-mRNA splicing (Ren et al., 2017). An RBP can also play multiple roles in mRNP metabolism, as with UAP56 which functions both in resolving co-transcriptionally formed R-loops and as a part of TREX complex (Pérez-Calero et al., 2020).

Gle1 modulates the activity of several DBPs at different stages in the mRNA life cycle (Aryanpur et al., 2017; Bolger et al., 2008; Bolger and Wente, 2011; Folkmann et al., 2011). In humans, at least two isoforms of Gle1 (Gle1A and Gle1B) arise through alternative splicing of the *GLE1* gene (Kendirgi et al., 2003) and perform distinct functions. Both isoforms shuttle between the nucleus and cytoplasm via a 39 amino acid shuttling domain (herein termed Gle1-SD) (Kendirgi et al., 2003), and share other functional domains, including an amino (N)-terminal Nup155 binding domain, low complexity and coiled-coil domains required for oligomerization, and a carboxy (C)-terminal domain that interacts with DDX19 and inositol hexakisphosphate (IP_6) (Adams et al., 2017; Kendirgi et al., 2003; Mason and Wente, 2020). The two isoforms are only differentiated by an addition of 43 amino acids at the C-terminus of Gle1B, which mediate binding to hCG1 at the NPC (Adams et al., 2017). Interaction with hCG1 enables Gle1B localization at the cytoplasmic face of the nuclear pore complex (NPC) and function in mRNP remodeling during the terminal steps of mRNA export. Our laboratory has methodically defined key steps in the mRNA export mechanism whereby Nup42 and IP_6 stimulate Gle1-mediated activation of DDX19 (*S. cerevisiae* Dbp5) during mRNA export (Adams et al., 2017; Folkmann et al., 2013; Lin et al., 2018). Recently, Gle1 was also shown to modulate tRNA export through activation of Dbp5 (Rajan et al., 2023).

In addition to the role for Gle1B in mRNA export at the NPC, Gle1B also functions in the nucleus during transcriptional termination (Sharma and Wente, 2020). We recently established that the Gle1-SD is necessary for coordinating DDX1 and Cstf-64 for pre-mRNA cleavage of specific poly(A)+ RNAs. When Gle1 shuttling is abrogated, the interaction between the DDX1 and Cstf-64 complex within transcription termination machinery is disrupted. Consequently, pre-mRNA cleavage is not executed at the transcription termination sequence, resulting in elongated 3’UTR and the formation of R-loops (Sharma and Wente, 2020).

In contrast, the Gle1A isoform has specific cytoplasmic roles which are associated with cellular stress responses. Work in *S. cerevisiae* has shed light on the multifunctional role that cytoplasmic Gle1 plays in modulating Ded1 (human DDX3) functions during translation

initiation (Aryanpur et al., 2017; Bolger and Wente, 2011). During stress conditions in human cells, global translation is halted and pre-existing mRNPs assemble into stress granules (SGs) through a dynamic process that is dependent on Gle1A and DDX3 (Aditi et al., 2016; Glass and Wente, 2019). Additionally, in response to cellular stress, the N-terminal domain Gle1A is hyperphosphorylated near its low complexity domain by ERK, JNK and GSK3. Basal levels of Gle1 phosphorylation promote self-association of Gle1A and formation of mature SGs. Gle1A becomes hyperphosphorylated during stress recovery, perturbing its self-association and leading to disassembly of SGs and resumption of translation (Aditi et al., 2019; Mason and Wente, 2020). Thus, phosphorylation of Gle1 is a key aspect of temporal regulation for mRNAs during stress conditions.

In this study, we generated antibodies that are specific for Gle1 phosphorylated at threonine 102 (anti-Gle1-pT102). Interestingly, we discovered that Gle1-pT102 is predominantly nuclear but under stress conditions becomes more localized to the cytoplasm. We also found that association between Gle1-pT102 and DDX1 increased when nucleocytoplasmic shuttling of Gle1 decreased. These studies suggest that distribution of Gle1 is impacted by its phosphorylation state and potentially plays a role in nuclear Gle1 functions.

Materials and Methods

Phosphospecific Gle1 Antibody Production:

Phosphorylation specific Gle1 antibodies for threonine 102 (ASW58 and ASW59) were generated by Pacific Immunology (Ramona, CA). Pacific Immunology synthesized the peptide antigen Gle1-P (97pT102 −108): PASPA-pTpPNGTKG-Cys and coupled to Keyhole Limpet Hemocyanin via the terminal Cys (Figure 1A). A non-phosphorylated peptide Gle1-NP (97–108): PASPATPNGTKG-Cys was also synthesized (Figure 1A). The Gle1-P coupled peptide was used for four immunizations of two New Zealand white rabbits over 13 weeks. Serum was affinity purified by the manufacturer against the non-phosphorylated peptide (ASW59) with the flow-through being purified against the phosphorylated peptide (ASW58). Antibodies were snap frozen in liquid nitrogen in PBS with 0.02% sodium azide without significant loss of function. ASW58 and ASW59 were used for immunoblotting, immunofluorescence, and immunoprecipitation, with ASW59 being of higher titer for Gle1-pT102. Other previously published antibodies used in this study include: ASW47.1 (rabbit anti-human Gle1, (Mason and Wente, 2020)), ASW48 (guinea pig anti-human $Gle1^{1-360}$, (Aditi et al., 2015)); anti-DDX1 (mouse anti-human DDX1 monoclonal, Novus Biologicals (Sharma and Wente, 2020)), goat anti-guinea pig IgG Alexa Fluor 488 (Invitrogen), goat anti-rabbit IgG Alexa Fluor 568 (Invitrogen).

Total Cell Lysate Production:

HeLa cells were plated on 10cm dishes. Following the indicated treatment, cells were lysed in 50 mM Tris-HCl pH 7.5, 150 mM NaCl, 1.5 mM $MgCl_2$, 1% NP-40 and 1x cOmplete EDTA-free protease inhibitor (Merck). Supernatant was cleared by centrifugation at 13,000 rpm for 10 min at 4°C. Equal volumes of cell lysates were incubated at 30°C for 30 mins with 1X NEBuffer for MettaloPhosphatases (NEB) and 1 mM $MnCl_2$ alone or with the addition of lambda phosphatase in the absence or presence of 1x PhosSTOP

(Sigma-Aldrich). Reactions were terminated by the addition of 6x Laemmli buffer and analyzed by immunoblotting.

Protein purification:

Plasmids expressing MBP-Gle1$^{1-360,\ T102A}$ and MBP-Gle1$^{1-360,\ 5A\ T102}$ were generated by altering plasmids expressing MBP-Gle1$^{1-360}$ (pSW4392) and MBP-Gle1$^{1-360,\ 6A}$ (pSW4396) (Aditi et al., 2019), respectively, with the QuikChange Lightning Site-directed mutagenesis kit (Agilent) according to the manufacturer's directions. Maltose Binding Protein (MPB)-Gle1$^{1-360}$, MBP-Gle1$^{1-360,\ T102A}$, MBP-Gle1$^{1-360,\ 5A\ T102}$, and Gle1$^{1-360,6A}$ fusion proteins were purified as described previously (Aditi et al., 2019). Briefly, *E.coli* Rosetta cells transformed with respective expression plasmids were cultured in Terrific Broth under kanamycin and chloramphenicol selection. Expression was induced with 0.2 mM isopropyl 1-thio-D-galactopyranoside at an A_{600} of 0.8 for 18 hrs at 18°C. Bacteria were lysed by sonication in 20 mM HEPES (pH 7.5), 500 mM NaCl, 0.5 mM TCEP, and 20% glycerol supplemented with cOmplete EDTA-free protease inhibitor (Merck) mixture and 2 mM PMSF. Cleared lysates were batch bound with amylose resin equilibrated in above buffer for 2 hrs followed by a 20 column volume wash. Proteins were eluted with the addition of 10 mM maltose. Proteins were buffer exchanged and concentrated into buffer containing 20 mM HEPES (pH 7.5), 200 mM NaCl, 0.5 mM TCEP and 20% glycerol.

In-vitro phosphorylation assay:

Recombinant bacterially produced proteins (4 μg) were incubated with 100 units of ERK enzyme (New England Biolabs (NEB)), 100 ng of JNK enzyme (Thermo Scientific), and 125 units of GSK-3 (NEB) as indicated for 30 mins at 30°C in 40 μl reactions with manufacturer supplied kinase reaction buffer (NEB) supplemented with ATP to a final concentration of 100 μM. Reactions were stopped by addition of 6x Laemmli buffer and heated at 95°C for 5 mins. Samples were analyzed by immunoblotting.

Immunoprecipitation:

Confluent HeLa cells plated in T75 flasks were treated with 0.5 mM sodium arsenite or left untreated for 60 minutes. Cells were lysed in 20 mM Tris-HCl (pH 7.5), 150 mM NaCl, 2mM $MgCl_2$, 1mM EDTA, 0.5% NP-40, and cOmplete EDTA-free protease inhibitor (Merck). Samples treated lambda phosphatase were adjusted with $MnCl_2$ and incubated at room temperature for 30 mins. To the 500 μl samples, 16 μl of ASW59 was added and incubated overnight with rotation at 4°C. Protein A–Sepharose beads (Cytiva) that were pre-blocked with lysis buffer plus 5% BSA, were added to the antibody/lysate mixture and incubated for 2 hrs at 4°C with rotation. The beads were washed 5x with lysis buffer and after final wash, resuspended with 40μl of 3x Laemmli buffer and heated to 95°C for 5 mins.

Immunofluorescence:

HeLa cells (<12 passages) were plated and grown overnight on coverslips in a 24-well tray (2.5×10^5 cells per well). Cells were treated with 0.5 mM of sodium arsenite for 1 hour or 5 μM Gle1-scr or SD peptide (Kendirgi et al., 2003) for 4 hours at 37°C, 5% CO_2

(as indicated). Cells were fixed with 100% chilled methanol at −20°C for 5 mins, washed three times with 70% chilled ethanol for 5 mins on ice followed by 1xPBS washes. Cells were blocked with 50 mg/ml BSA, 0.2% Triton-X-100, 2% normal goat serum in 1xPBS for overnight at 4°C in a humidified chamber. Primary antibodies were diluted in blocking buffer and incubated overnight at 4°C in a humidified chamber. Cells were washed with 1xPBS and immunostained with anti-Gle1-pT102 (ASW59) and anti-DDX1 antibodies and visualized with AF-488 and AF-594 secondary antibodies respectively. Cells were washed with 1xPBS, incubated with NucRed (ThermoFisher) (diluted in PBS) for 45 mins at RT and mounted in Vectashield (Vector Laboratories). Slides were imaged using 63× 1.4 NA or 100× 1.47 NA objective on a Leica SP5 confocal microscope. Post-image analysis was done using ImageJ software. GraphPad Prism software was used to graph the data and calculate statistical significance.

Proximity Ligation Assay and analyses:

Duolink PLA (Sigma-Aldrich) fluorescence protocol was followed with following changes. HeLa cells were plated on an 8-well chamber slide (2×10^4 cell per chamber), treated (as indicated), fixed and blocked overnight at 4°C in a humidified chamber with the same blocking buffer as used for immunofluorescence (see above). Primary antibodies were diluted in the immunofluorescence blocking buffer overnight at 4°C in a humidified chamber. Slides were washed and processed exactly as outlined in the manufacturer's instructions. Cells were counter-stained with NucRed for 45 mins prior to mounting and image on Leica SP5 confocal microscope with 100x oil objective. Images were processed and analyzed on ImageJ software.

Results and Discussion

Phospho-Gle1 antibody specifically recognizes Thr102 phosphorylated Gle1:

In our previous studies (Aditi et al., 2019; Glass and Wente, 2019) we found that Gle1 is phosphorylated under stress conditions such as during heat shock and with sodium arsenite treatment. To further analyze the function of phosphorylated Gle1, a rabbit anti-serum was produced using a 13 amino acid peptide antigen spanning from residue 97 to 108 of Gle1 with Thr 102 phosphorylated (Gle1-P; Figure 1A). The affinity-purified antibodies (ASW58 and ASW59) were tested for specificity by immunoblotting with lysates from HeLa cells that were either untreated or treated with sodium arsenite. A parallel blot was probed with ASW47.1 antibody that recognizes total Gle1 (Mason and Wente, 2020). Immunoblot analyses revealed that ASW58 recognizes Gle1 (Figure 1B, left panel, compare lane 1 and 4). ASW59 also recognizes Gle1; however, some background proteins are detected at a low level (Figure 1B, right panel, compare lane 1 and 4). To determine whether the protein recognized by ASW58 and ASW59 was phosphorylated, HeLa cell lysates were treated with lambda phosphatase with or without phosphatase inhibitor. Immunoblot analyses revealed that the slower mobility band collapses in the presence of lambda phosphatase (Figure 1B, compare lanes 4 and 5) while this shift is abrogated in the presence of phosphatase inhibitor (Figure 1B compare lanes 5 and 6). These results showed that ASW58 and ASW59 specifically recognize stress-induced, phosphorylated Gle1 from HeLa cell lysates. The

generation of antibodies recognizing a phospho-specific form of Gle1 provides a key tool for analyzing phosphorylated Gle1 function.

We reported in published studies that the MAPK family kinases ERK and JNK phosphorylate Gle1 in its N-terminal region to then allow further GSK3-mediated phosphorylation (Aditi et al., 2019). To test the specificity of ASW58 and ASW59 for recognizing Gle1 phosphorylated at Thr102, we conducted *in-vitro* phosphorylation assays. Bacterially expressed MPB-Gle1 fusion protein for the first N-terminal 360 residues of Gle1 (MPB-Gle1$^{1-360}$) was purified and incubated with or without purified active ERK and JNK in the presence of ATP. In the absence of ERK and JNK, the non-phosphorylated MPB-Gle1$^{1-360}$ was not recognized by ASW59 (Figure 2A, middle panel, lane 1) or by ASW58 (Figure 2A, bottom panel, lane 1). Immunoblotting with ASW47.1 (recognizing total Gle1) verified the presence of protein (Figure 2A, top panel). When the MPB-Gle1$^{1-360}$ protein was incubated with the MAPK kinases ERK and JNK, it was detected by both the ASW59 (Figure 2A, middle panel, lane 2) and ASW58 antibodies (Figure 2A, bottom panel, lane 2). In contrast, when the six phosphorylation sites in the N-terminal region were replaced with alanine residues (including Thr102) (Aditi et al., 2019), the MPB-Gle1$^{1-360,6A}$ sample incubated with ERK/JNK did not show detectable Gle1 with either ASW59 or ASW58 (Figure 2A, middle and bottom panels respectively, lane 4). Thus, ASW58 and ASW59 specifically recognize phosphorylated Gle1.

Taking this further and to test for specific recognition of phosphorylated Thr102, two different MPB-Gle1$^{1-360}$ variants were compared to wild-type: MPB-Gle1$^{1-360,T102\ A}$ where Thr102 was replaced by Ala, and MPB-Gle1$^{1-360,\ 5A\ T102}$ where all five Ser residues (S88, S92, S93, S96, and S99) were changed to Ala. With MPB-Gle1$^{1-360\ T102A}$, after incubation with ERK, JNK, and GSK either singularly or all three in combination, the protein was not detected with ASW58 (Figure 2B, left panel, lane 7, 8, 9 and 10). Conversely, MPB-Gle1$^{1-360\ 5A\ T102}$ was detected after incubation with ERK or JNK, or with ERK/JNK and GSK. (Figure 2B, right panel, lanes, 2, 3, and 5), but not with GSK alone (Figure 2B, right panel, lane 4). Immunoblotting with anti-MBP antibody confirmed equal protein loading (Figure 2B, left and right panels). These results verified that the ASW58 antibody specifically recognizes Gle1 phosphorylated at Thr102; referred to subsequently as Gle1-pT102. Further, the five Ser phosphorylation sites in the 1–360 region of Gle1 are not required for Thr102 phosphorylation. We speculate that Thr102 phosphorylation is a critical priming event for further phosphorylation of other residues in the low complexity N-terminal Gle1 domain.

Gle1-pT102 associates and co-locates with DDX1 in the nucleus:

We recently discovered a nuclear role of Gle1 in human cells (Sharma and Wente, 2020). In the nucleus, Gle1 functions in concordance with the DEAD-box RNA helicase, DDX1, and transcription termination machinery to cleave nascently transcribed RNA. To understand the subcellular localization of Gle1-pT102, indirect immunofluorescence microscopy studies were conducted. Untreated or sodium arsenite treated HeLa cells were fixed and co-immunostained with ASW59 (detects Gle1-pT012) and ASW48 (detects total Gle1) (Figure 2C). Interestingly, in untreated cells, Gle1-pT102 showed predominantly

nuclear distribution with a punctate pattern with some pan-cellular distribution through the cytoplasm. Gle1-pT102 did not show enrichment at the nuclear rim. Upon sodium arsenite stress, Gle1-pT102 colocalized with total Gle1 in cytoplasmic stress granules.

Given the nuclear localization of Gle1-pT102, we next tested for physical interactions between Gle1-pT102 and DDX1 in co-immunoprecipitation experiments. Lysates from untreated and sodium arsenite treated HeLa cells were processed for immunoprecipitation with ASW59 antibody. The total lysate (input) and bound fractions were then immunoblotted with anti-DDX1 antibody. As shown in Figure 3A, phosphorylated Gle1 interacts with DDX1 under non-stressed (lane 5) and stressed (lane 6) conditions. Treatment of the respective cell lysates with lambda phosphatase prior to immunoprecipitation (Figure 3A; lanes 7 and 8) resulted in no detectable co-isolation of DDX1 with anti-Gle1-pT102 antibodies. Based on this, we concluded that DDX1 preferentially interacts with phosphorylated Gle1 versus phosphatase treated Gle1.

The association between Gle1-pT102 and DDX1 was further analyzed by indirect immunofluorescence microscopy assays. A single slice from the z-stack stained with anti-Gle1-pT102 (ASW59) and anti-DDX1 antibodies is depicted in Figure 3B. Both proteins showed punctate localization patterns in the nucleus (nucRed) which distinctly overlap as observed in the merged panel (far right).

Next, association between Gle1-pT102 and DDX1 was tested by Proximity Ligation Assay (PLA) in HeLa cells, whereby an amplified signal is produced only if the two proteins bound by their respective antibodies are within 40nm distance (Che and Khavari, 2017; Greenwood et al., 2015). PLA signal was quantified from the maximum projected z-stacks as the number of PLA dots per nucleus, as well as nuclear fluorescence intensity (Integrated Density) (Figure 3C). Nuclear signal was quantified and plotted. The individual anti-Gle1-pT102 (ASW59) and anti-DDX1 antibodies generated very low background signals. Incubating HeLa cells with both the antibodies in this assay generated a strong signal over the background. Taken together, these results indicated that Gle1-pT102 and DDX1 proteins are closely associated in the nucleus.

Inhibiting Gle1 nucleocytoplasmic shuttling increases association of Gle1-pT102 with DDX1 in the nucleus:

Our prior study documented that Gle1 shuttles between the nucleus and cytoplasm via a 39 amino acid Shuttling Domain (SD) (Kendirgi et al., 2003). We also discovered that treatment of HeLa cells with a SD peptide inhibits the shuttling of endogenous Gle1 and decreases the level of Gle1 localization at NPC. We investigated if distribution of Gle1-pT102 changes upon treatment with Gle1-SD. HeLa cells were incubated with a control Gle1-scr peptide or the Gle1-SD peptide for 4 hours (as described in (Sharma and Wente, 2020)). Gle1-pT102 remained pre-dominantly nuclear after Gle1-SD treatment and no change in nuclear/cytoplasmic fluorescent intensity was observed at steady state levels (Figure 4A). It is interesting to note that the nucleocytoplasmic distribution of Gle1-pT102 did not change after Gle1-SD treatment whereas Gle1-pT02 relative localization appeared to be shift from the nucleus to cytoplasm after sodium arsenite stress (seen in Figure 2C). This

suggests a differential response of Gle1-pT102 under two different cellular conditions and future studies will be needed to test this hypothesis.

To investigate the association between Gle1-pT102 and DDX1 after Gle1-SD peptide treatment, the Proximity Ligation Assay was used. As shown in Figure 4B, the nuclear association of Gle1-pT102 with DDX1 increased upon Gle1-SD treatment. This is in contrast to the association between total Gle1 and DDX1 which is reduced significantly upon Gle1-SD treatment (Sharma and Wente, 2020). Based on these results, we concluded that Gle1-pT102 preferentially interacts with DDX1 in the nucleus.

Conclusion:

In this study, we generated antibodies that specifically recognize human Gle1 that is phosphorylated at Threonine residue 102. The specificity of the anti-Gle1-pT102 antibody was rigorously confirmed using *in vitro* phosphorylation assays. Using this antibody to investigate Gle1 in human cells, we found Gle1-pT102 co-immunoprecipitated with DDX1 from cell lysates in a phosphatase sensitive manner. Immunofluorescence studies revealed that Gle1-pT102 predominantly resides in the nucleus in a punctate distribution where it co-locates with DDX1. Under sodium arsenite stress conditions, Gle1-pT102 localization was pan-cellular and colocalized with stress granules as identified with total Gle1 staining. Treatment with Gle1-SD peptide, which inhibits the nucleocytoplasmic shuttling of endogenous Gle1 (Kendirgi et al., 2003) did not change the nuclear intensity or distribution of Gle1-pT102. Taken together, our results suggest that Gle1-pT102 has a reduced ability to shuttle between the nucleus and the cytoplasm.

We also found that Gle1-SD treatment increases the interaction between Gle1-pT102 and DDX1 in the nucleus. In our previous studies (Sharma and Wente, 2020), nuclear levels of DDX1 increase after Gle1-SD treatment but total Gle1-DDX1 interaction decreases. Considering the new results in this report and our prior studies together, we propose that Gle1-pT102 is retained by DDX1 in the nucleus. Overall, this study sheds novel insights into the dynamic and temporal distribution of Gle1-pT102 under cellular stress conditions.

Acknowledgements

These experiments were conducted while the authors were in the Department of Cell and Developmental Biology at the Vanderbilt University School of Medicine, and S.R.W. was the Cornelius Vanderbilt Chair. We are thankful to Aditi for useful discussions. This work was supported by the National Institutes of Health (NIH) Grant 5R37GM051219 (to S.R.W.). Microscopy was performed in part using the Vanderbilt Cell Imaging Shared Resource, supported by the National Institutes of Health grants CA68485, DK20593, DK58404, DK59637 and EY08126.

References

Adams RL, Mason AC, Glass L, Aditi, Wente, S.R., 2017. Nup42 and IP_6 coordinate Gle1 stimulation of Dbp5/DDX19B for mRNA export in yeast and human cells. Traffic 18, 776–790. 10.1111/tra.12526 [PubMed: 28869701]

Aditi Mason, A.C., Sharma M, Dawson TR, Wente SR, 2019. MAPK- and glycogen synthase kinase 3-mediated phosphorylation regulates the DEAD-box protein modulator Gle1 for control of stress granule dynamics. J Biol Chem 294, 559–575. 10.1074/jbc.RA118.005749 [PubMed: 30429220]

Aditi Folkmann, A.W., Wente SR, 2015. Cytoplasmic hGle1A regulates stress granules by modulation of translation. Mol Biol Cell 26, 1476–1490. 10.1091/mbc.E14-11-1523 [PubMed: 25694449]

Aditi Glass, L., Dawson TR, Wente SR, 2016. An amyotrophic lateral sclerosis-linked mutation in GLE1 alters the cellular pool of human Gle1 functional isoforms. Adv Biol Reg 62, 25–36. 10.1016/j.jbior.2015.11.001

Aryanpur PP, Regan CA, Collins JM, Mittelmeier TM, Renner DM, Vergara AM, Brown NP, Bolger TA, 2017. Gle1 Regulates RNA Binding of the DEAD-Box Helicase Ded1 in Its Complex Role in Translation Initiation. Mol Cell Biol 37, e00139–17. 10.1128/MCB.00139-17 [PubMed: 28784717]

Bléoo S, Sun X, Hendzel MJ, Rowe JM, Packer M, Godbout R, 2001. Association of human DEAD box protein DDX1 with a cleavage stimulation factor involved in 3'-end processing of pre-MRNA. Mol Biol Cell 12, 3046–3059. 10.1091/mbc.12.10.3046 [PubMed: 11598190]

Bohnsack KE, Yi S, Venus S, Jankowsky E, Bohnsack MT, 2023. Cellular functions of eukaryotic RNA helicases and their links to human diseases. Nat Rev Mol Cell Biol 10.1038/s41580-023-00628-5

Bolger TA, Folkmann AW, Tran EJ, Wente SR, 2008. The mRNA Export Factor Gle1 and Inositol Hexakisphosphate Regulate Distinct Stages of Translation. Cell 134, 624–633. 10.1016/j.cell.2008.06.027 [PubMed: 18724935]

Bolger TA, Wente SR, 2011. Gle1 Is a Multifunctional DEAD-box Protein Regulator That Modulates Ded1 in Translation Initiation. J Biol Chem 286, 39750–39759. 10.1074/jbc.M111.299321 [PubMed: 21949122]

Chakraborty P, Huang JTJ, Hiom K, 2018. DHX9 helicase promotes R-loop formation in cells with impaired RNA splicing. Nat Commun 9, 4346. 10.1038/s41467-018-06677-1 [PubMed: 30341290]

Che Y, Khavari PA, 2017. Research Techniques Made Simple: Emerging Methods to Elucidate Protein Interactions through Spatial Proximity. J Invest Dermatol 137, e197–e203. 10.1016/j.jid.2017.09.028 [PubMed: 29169465]

Folkmann AW, Collier SE, Zhan X, Aditi Ohi MD, Wente SR 2013. Gle1 functions during mRNA export in an oligomeric complex that is altered in human disease. Cell 155, 582–593. 10.1016/j.cell.2013.09.023 [PubMed: 24243016]

Folkmann AW, Noble KN, Cole CN, Wente SR, 2011. Dbp5, Gle1-IP_6 and Nup159: a working model for mRNP export. Nucleus 2, 540–548. 10.4161/nucl.2.6.17881 [PubMed: 22064466]

Glass L, Wente SR, 2019. Gle1 mediates stress granule-dependent survival during chemotoxic stress. Adv Biol Regul 71, 156–171. 10.1016/j.jbior.2018.09.007 [PubMed: 30262214]

Greenwood C, Ruff D, Kirvell S, Johnson G, Dhillon HS, Bustin SA, 2015. Proximity assays for sensitive quantification of proteins. Biomol Detect Quantif 4, 10–16. 10.1016/j.bdq.2015.04.002 [PubMed: 27077033]

Kendirgi F, Barry DM, Griffis ER, Powers MA, Wente SR, 2003. An essential role for hGle1 nucleocytoplasmic shuttling in mRNA export. J Cell Biol 160, 1029–1040. 10.1083/jcb.200211081 [PubMed: 12668658]

Lin DH, Correia AR, Cai SW, Huber FM, Jette CA, Hoelz A, 2018. Structural and functional analysis of mRNA export regulation by the nuclear pore complex. Nat Commun 9, 2319. 10.1038/s41467-018-04459-3 [PubMed: 29899397]

Mason AC, Wente SR, 2020. Functions of Gle1 are governed by two distinct modes of self-association. J Biol Chem 295, 16813–16825. 10.1074/jbc.RA120.015715 [PubMed: 32981894]

Mersaoui SY, Yu Z, Coulombe Y, Karam M, Busatto FF, Masson J-Y, Richard S, 2019. Arginine methylation of the DDX5 helicase RGG/RG motif by PRMT5 regulates resolution of RNA:DNA hybrids. EMBO J 38, e100986. 10.15252/embj.2018100986 [PubMed: 31267554]

Natalizio BJ, Wente SR, 2013. Postage for the messenger: designating routes for nuclear mRNA export. Trends Cell Biol 23, 365–373. 10.1016/j.tcb.2013.03.006 [PubMed: 23583578]

Pérez-Calero C, Bayona-Feliu A, Xue X, Barroso SI, Muñoz S, González-Basallote VM, Sung P, Aguilera A, 2020. UAP56/DDX39B is a major cotranscriptional RNA-DNA helicase that unwinds harmful R loops genome-wide. Genes Dev 34, 898–912. 10.1101/gad.336024.119 [PubMed: 32439635]

Rajan AAN, Asada R, Montpetit B, 2023. Gle1 is required for tRNA to stimulate Dbp5 ATPase activity in vitro and to promote Dbp5 mediated tRNA export in vivo (preprint). Molecular Biology 10.1101/2023.06.29.547072

Ren Y, Schmiege P, Blobel G, 2017. Structural and biochemical analyses of the DEAD-box ATPase Sub2 in association with THO or Yra1. Elife 6, e20070. 10.7554/eLife.20070 [PubMed: 28059701]

Sharma M, Wente SR, 2020. Nucleocytoplasmic shuttling of Gle1 impacts DDX1 at transcription termination sites. Mol Biol Cell 31, 2398–2408. 10.1091/mbc.E20-03-0215 [PubMed: 32755435]

Skourti-Stathaki K, Proudfoot NJ, Gromak N, 2011. Human senataxin resolves RNA/DNA hybrids formed at transcriptional pause sites to promote Xrn2-dependent termination. Mol Cell 42, 794–805. 10.1016/j.molcel.2011.04.026 [PubMed: 21700224]

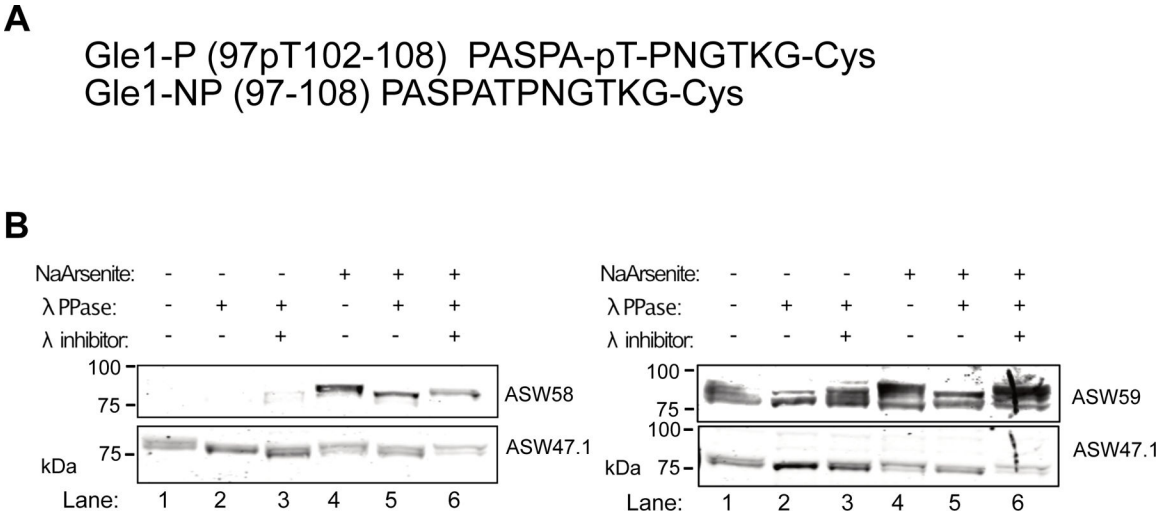

Figure 1:

ASW58 and ASW59 recognize phosphorylated Gle1. **(A)** Gle1 peptide sequence Gle1-P, with phosphorylated Threonine residue 102, used for generation of anti-Gle1-pT102 antibodies, ASW58 and ASW59. **(B)** Following treatment with sodium arsenite or no treatment for 1 hour, HeLa cells were lysed with 1% NP-40 buffer and supernatant was treated lambda phosphatase +/− inhibitor as indicated. Immunoblots were probed with ASW47.1, ASW58 (left panel), and ASW59 (right panel) antibodies.

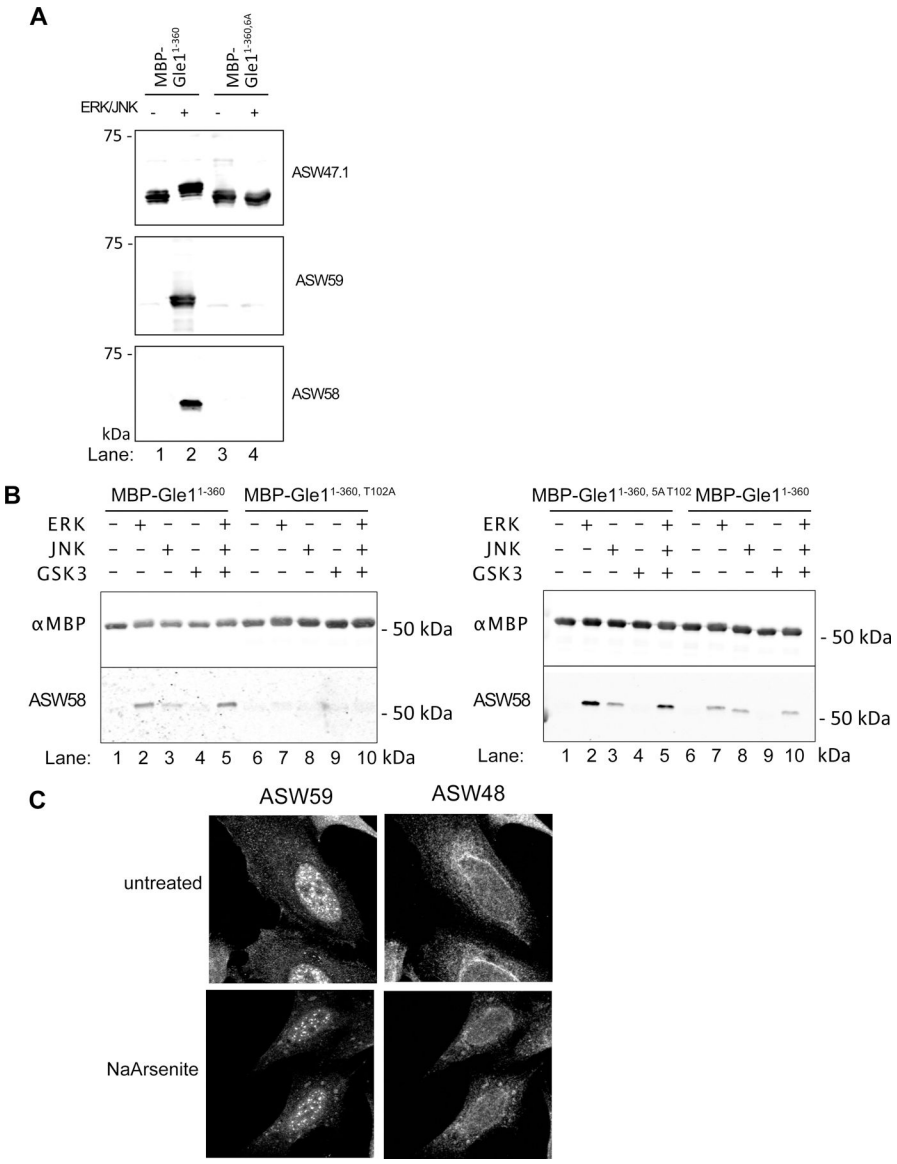

Figure 2:

ASW58 and ASW59 antibodies are specific for Gle1 Thr102 phosphorylation. **(A)** MBP-Gle1$^{1-360}$ and MBP-Gle1$^{1-360,\ 6A}$ were incubated in the presence or absence of ERK and JNK. Phosphorylation was detected by immunoblotting with ASW59 and ASW58, while total Gle1 protein was detected with ASW47.1. **(B)** MBP-Gle1$^{1-360}$, MBP-Gle1$^{1-360,\ 5A\ T102}$, and MBP-Gle1$^{1-360,\ T102A}$ were incubated in the presence of ERK, JNK, and GSK3 separately, together, and in the absence of any kinase. Total Gle1 protein was detected by immunoblotting with anti-MBP and phosphorylated Gle1 was detected with ASW58. **(C)** HeLa cells were either treated with sodium arsenite or left untreated. Cells were co-immunostained with ASW59 (anti-Gle1-pT102) and ASW48 (total Gle1) primary antibodies and goat anti-rabbit IgG Alexa Fluor 568 and goat anti-guinea pig IgG Alexa Fluor 488 secondary antibodies, respectively showing differences in Gle1 distribution at steady state and localization into stress granules upon sodium arsenite treatment.

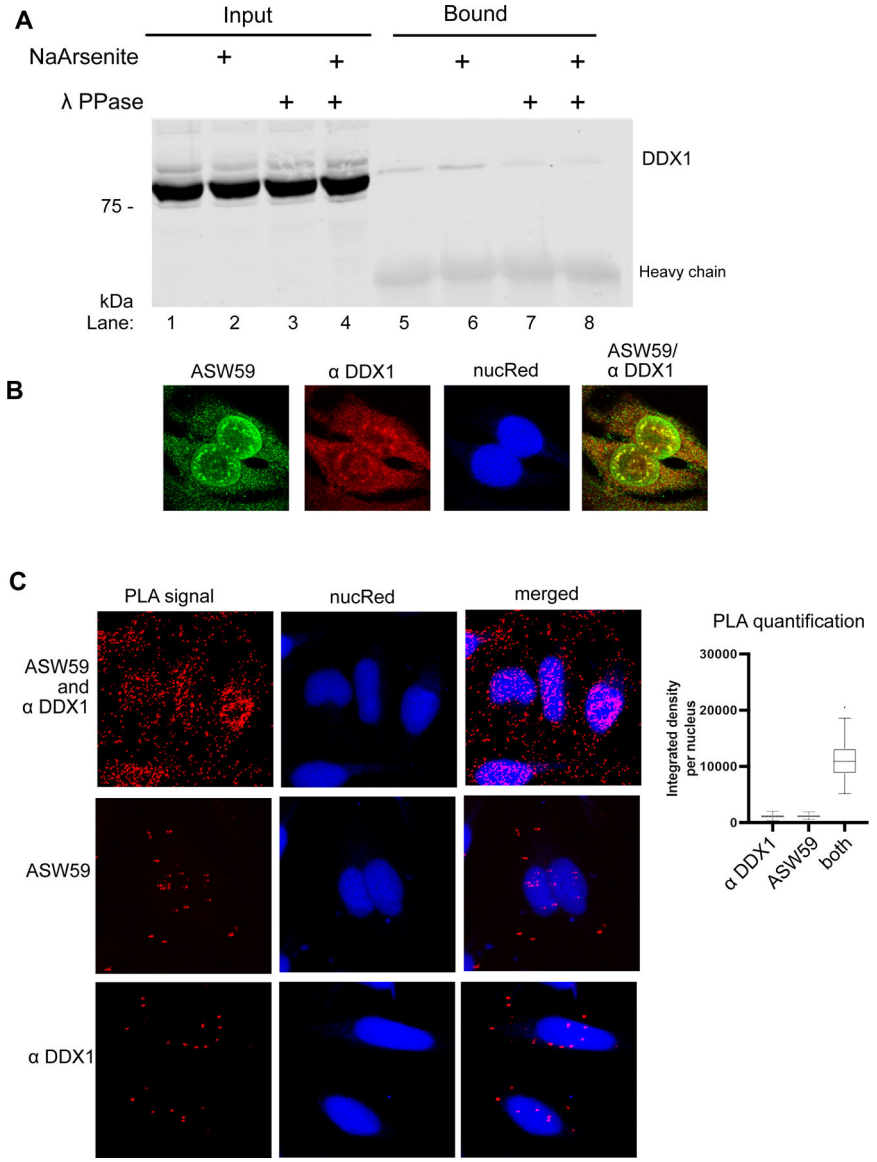

Figure 3:

Gle1-pT102 associates and colocalizes with DDX1. **(A)** HeLa cells were either left untreated or treated with sodium arsenite for 60 min. Cell lysates were then incubated in the presence or absence of lambda phosphatase and immunoprecipitated with ASW59 (anti-Gle1-pT102) and immunoblotted with anti-DDX1. **(B)** HeLa cells were co-immunostained with ASW59 (anti-Gle1-pT102), anti-DDX1 and detected with goat anti-rabbit IgG Alexa Fluor 488 and goat anti-mouse IgG Alexa Fluor 568. The nucleus was detected with nucRed. **(C)** Proximity Ligation Assay depicting colocalization between ASW59 (anti-Gle1-pT102) and anti-DDX1 which is quantified in the right panel. Images were captured on Leica SP5 confocal microscope using 100x objective.

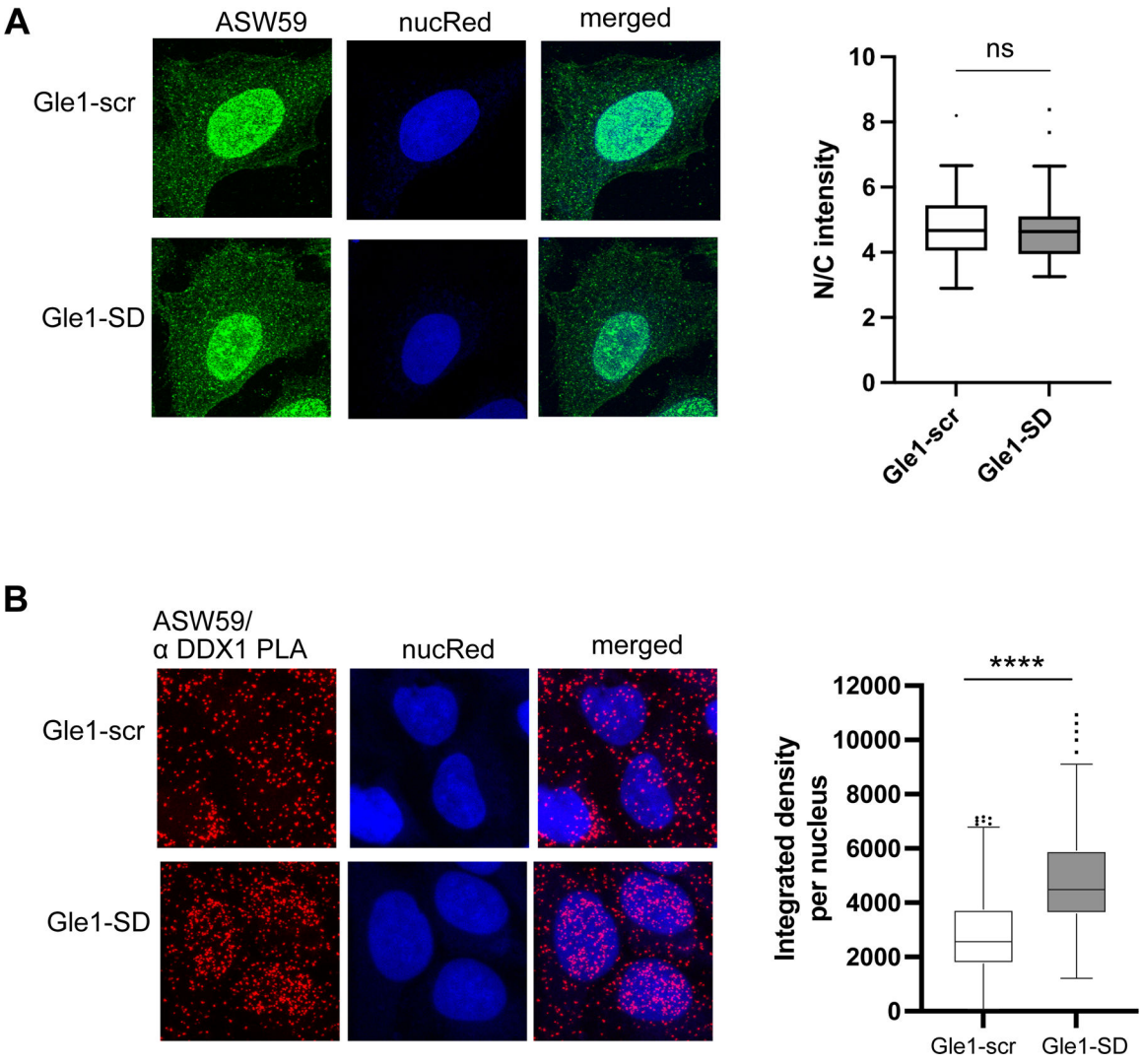

Figure 4:

Gle1-SD treatment increases association between Gle1-pT102 and DDX1. **(A)** HeLa cells were treated with Gle1-scr or SD peptide and immunostained with ASW59 (anti-Gle1-pT102) and nucRed followed by imaging on a confocal microscope. Maximum intensity projected images were quantified for nuclear and cytoplasmic intensities using ImageJ and graphed using Prism software. **(B)** HeLa cells were treated with Gle1-scr or SD peptide followed by Proximity Ligation Assay (left panel). Integrated density in the nucleus was quantified on maximum intensity projected images using ImageJ (right panel); ns=not significant and ****p<0.005 Images were captured on Leica SP5 confocal microscope using 100x objective.